Journal of Materials Chemistry C

Accepted Manuscript

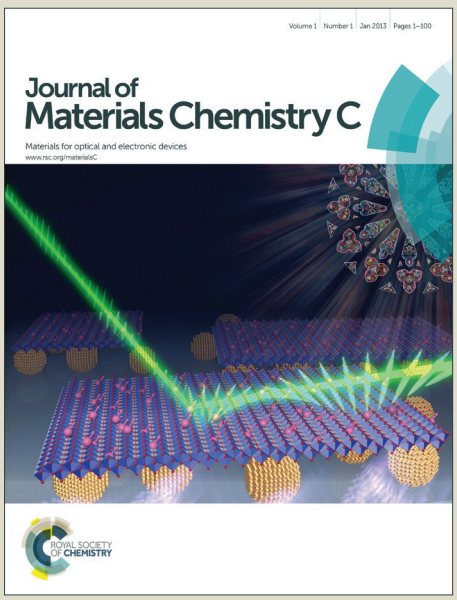

ROYAL SOCIETY OF CHEMISTRY

www.rsc.org/materialsC

Fabrication of Flexible Microlens Arrays through Vapor-induced Dewetting on Selectively Plasma-treated Surfaces

Xiaopeng Bi, Wen Li[*]

Microtechnology Laboratory, Department of Electrical and Computer Engineering, Michigan State University, East Lansing, MI 48824 USA

Abstract

Microlens arrays have been increasingly employed as key components in building micro-optical systems. Conventional fabrication methods, such as grayscale lithography, ink-jet printing, and photoresist thermal reflow, are often constricted by certain drawbacks, including mask resolution, high fabrication cost, and complexity of processes. In this paper, we present a low-temperature dewetting method that enables fabrication of microlens arrays on polymeric surfaces in a rapid and cost-effective way. As the demonstration of such a technique, vapor-induced dewetting of SU-8 thin films has been carried out on heterogeneous polydimethylsiloxane (PDMS) substrates that were selectively pre-treated with low-energy sulfur hexafluoride (SF_6) or oxygen (O_2) plasma. The dewetted SU-8 droplets are self-organized to directly form well-aligned microlens arrays on the O_2-plasma-treated regions, with various lens curvatures ranging from ~27 ° to ~47 ° as the processing temperature rises from 20 °C to 80 °C. The exposure to the solvent vapor allows for the realization of dewetting at low temperatures. The optical performance of such microlens arrays has been characterized by testing their imaging capabilities.

***Key words*:** Microlens array, Dewetting, Plasma treatment, SU-8, Polydimethylsiloxane

I. Introduction

Microlens arrays have been widely used as essential components in many optical systems, including digital display [1], integral imaging [2, 3], high-density data storage [4], and optical communications [5]. In particular, due to the capability of improving light out-coupling efficiency, the integration of microlens arrays with micro-light-emitting diodes (μ-LEDs) has become a promising solution to implanting light sources for applications that require high-resolution multisite illumination: for example, the rapidly progressing field of optical neural stimulation [6].

A variety of strategies have been developed for fabricating microlens arrays. Technically, they can be classified into two categories: photolithographic [7-10] and surface-tension-assisted [11-14] technologies. The former applies improved photolithographic methods to adjust the profile of ultraviolet (UV) light distribution and directly create 3-D microlens patterns on photoresists through a single exposure. For example, Totsu et al. employed a unique grayscale mask with a transmission gradient to generate a microlens array through photolithography [7]. Manevich et al. proposed using gap photolithography with an optimized distance between the photoresist film and the illuminated mask surface to make microlens arrays [8]. Hung et al. applied UV proximate printing and advanced optimization to fabricate a high fill-factor microlens array [9]. Wu et al. reported an improved femtosecond induced two-photon photo-polymerization technology for the production of closed-packed high numerical aperture microlens arrays [10]. However, some optical issues, such as mask resolution and light scattering, greatly limit the quality of microlenses fabricated by such methods. On the other hand, surface-tension-assisted technologies, such as the most commonly used ink-jet printing and photoresist thermal reflow methods, take advantage of surface tension to form spherically shaped microlenses with smooth profiles. Ink-jet printing, frequently operated in the drop-on-demand (DOD) mode, is a highly automated process with which patterns of microlenses can be written directly onto a substrate by dispensing droplets of an optical material at target positions [11-13]. Nevertheless, the difficulty of aligning microlenses on pre-patterned substrates is a

major obstacle. In the approach of photoresist thermal reflow, photoresist micro-cylinders are first created by conventional photolithography and subsequently baked above the glass transition temperature (T_g) of the photoresist to transform the cylindrical shape into the spherical lens shape through reflow [14]. Micro-printing or reactive ion etching (RIE) is often followed for lens replication to transfer the microlens profile into other materials with appropriate optical properties. However, besides high processing temperatures, the complexity of multi-step fabrication could affect the repeatability and yield of production.

Dewetting is another surface-tension-assisted technology that has been considered as one of the most promising strategies in surface patterning [15-17]. The dewetting process is driven by the minimization of surface energy and typically occurs at the solid-liquid interface [18]. An initially uniform film of a liquid breaks up, retracts, and eventually transforms into isolated droplets on a solid substrate. A liquid coating is thermodynamically unstable on a substrate if the spreading coefficient is negative [19], in which case dewetting can be triggered. However, due to lack of mobility, the dewetting phenomenon does not always occur on highly viscous polymer liquid films at room temperature. Thermal annealing above T_g of polymers is commonly used to activate the dewetting by increasing the mobility of polymer chains [16, 20, 21]. In an ordinary dewetting process that takes place on a flat and homogeneous substrate, a random distribution of ramified droplets is usually generated at the late stage, which is a major limitation for many applications. Therefore, advanced technological approaches are particularly desired in order to control the location of dewetted structures and create well-aligned microlens arrays. Several research groups have demonstrated that topological patterning on substrates is able to modulate the organization of dewetted structures [22-25]. Some groups have prepared chemically patterned substrates with periodic surface energy contrast to induce 1-D pattern-directed dewetting and thus roughly confine the final droplets [26, 27]. However, these methods cannot precisely control the position of dewetted droplets, which could greatly increase the difficulty of successive integrations. Although significant efforts have been devoted to the development of advanced approaches and mechanisms of dewetting [22-35], there

have been few dewetting experiments on chemically patterned surfaces for the fabrication of self-organized and well-aligned microlens arrays.

In this paper, we present a simple, rapid and cost-effective approach to fabricating microlens arrays on polymeric surfaces. Vapor-induced dewetting of SU-8 thin films has been carried out on biocompatible heterogeneous polydimethylsiloxane (PDMS) substrates that were selectively pre-treated with low-energy sulfur hexafluoride (SF_6) or oxygen (O_2) plasma. The employment of such plasma pre-treatments enables the self-confinement of dewetted SU-8 droplets within the O_2-plasma-treated regions, which is in good agreement with the numerical simulation. The exposure to the solvent vapor allows for the activation of dewetting at room temperature, which benefits the integration of materials and components that cannot stand a high temperature. The influences of film thickness and processing temperature on the microlens curvature have been studied experimentally. The optical performance of the as-fabricated microlens arrays has been characterized by testing their imaging capabilities.

II. Design and Methodology

2.1 Theory and Simulation

As a preliminary study, a numerical simulation was first performed to examine the dewetting process on an ordered, chemically heterogeneous substrate by using a lubrication-based computational model [36]. The thickness profile of the liquid film is represented by the function $h(x, y, t)$, where x and y are spatial coordinates and t is the time. The liquid film is assumed to be non-volatile so there is no volume loss during the dewetting process. Based on the conservation of volume, the evolution of the film thickness h is governed by the continuity equation:

$$\frac{\partial h}{\partial t} = -\nabla \cdot Q \,, \tag{1}$$

where Q denotes the horizontal flux and $\nabla\cdot$ is the two-dimensional divergence. Applying the lubrication approximation (i.e., slow-flow and small-slope) to the Navier-Stokes equation, Q is proportional to the pressure gradient, expressed by [37]:

$$Q = -\frac{h^3}{3\mu}\nabla p\,, \tag{2}$$

where μ is the dynamic viscosity, which is assumed to be constant across the thin liquid film. The pressure p includes capillary, gravitational and disjoining contributions:

$$p = -\sigma\nabla^2 h + \rho g h - \Pi\,, \tag{3}$$

in which σ is the surface tension, ρ is the density, g is the acceleration of gravity, and Π presents the so-called disjoining pressure with a widely-used form introduced by Schwartz and Eley [36]:

$$\Pi = \frac{(n-1)(m-1)}{h_0(n-m)}\sigma(1-\cos\theta)\left[\left(\frac{h_0}{h}\right)^n - \left(\frac{h_0}{h}\right)^m\right], \tag{4}$$

describing the interaction of the liquid with the substrate. Here, h_0 is the characteristic thickness, which is very small compared to the average thickness of the dewetting film and typically in the range of 1 to 100 nm [36]. n and m are positive constants with $n > m > 1$. Therefore, Π is governed by a long-range attractive potential and a short-range repulsive potential. $\theta(x, y)$ denotes the equilibrium contact angle and its position dependence represents the heterogeneity on the substrate. Combining Eqs. (1) to (4) yields the final form of the fourth-order non-linear evolution equation for the thickness profile:

$$h_t = -\nabla\cdot\left[-\frac{h^3}{3\mu}\nabla\left(-\sigma\nabla^2 h + \rho g h - \frac{(n-1)(m-1)}{h_0(n-m)}\sigma(1-\cos\theta)\left[\left(\frac{h_0}{h}\right)^n - \left(\frac{h_0}{h}\right)^m\right]\right)\right]. \tag{5}$$

The computational domain is sketched in Figure 1(a), which includes a 3 × 3 array of hydrophilic circular patterns with a diameter of 120 μm and a pitch of 250 μm on a hydrophobic substrate. Such specific

geometry was chosen to model the pattern dimension on the photomask, which will be employed in the experiment later. The contact angles on circular patterns and remaining substrate were set to 0.1 rad and 0.5 rad, respectively. The liquid properties μ = 0.0699 Pa·s, σ = 0.0334 N/m, and ρ = 1.075 g/mL corresponded to the actual value of SU-8 3005 (MicroChem Corp.). In addition, parameters (n, m, h_0) = (3, 2, 50 nm) were used in this study.

Eq. (5) was solved numerically using a finite-element algorithm by applying the alternating direction implicit (ADI) scheme and Newton's method (second-order Crank-Nicolson scheme) [38]. Nonlinear factors were evaluated at the previous time level. A 200 × 200 mesh was used with a mesh size of 3.75 μm, and an adaptive time-stepping procedure was employed to increase the computational efficiency. The initial condition included a liquid film with a uniform thickness of 1 μm and an introduced dry spot. Symmetry conditions were applied along all boundaries to simulate an ideal infinite array. The 3-D simulation result is shown in Figure 1(b). As can be seen, a self-organized microlens array was formed on the final profile, occupying the ordered hydrophilic areas as expected. This simulation provides qualitative guidance for the following fabrication technology.

2.2 Methods to Generate Heterogeneity

The nature of wetting on a surface is of crucial importance in the dewetting behavior of liquid thin films. In our experiment, polymeric substrates with heterogeneous surface wettability were first created using a low-energy plasma treatment in order to induce the self-organization of microlenses in the subsequent dewetting process. Based on our previous study, plasma treatment offers a facile route to alter the surface wettability [39, 40]. It can modify only the most external molecular layers of the material without affecting the bulk property. The SF_6 and O_2 plasma treatments have been found to be effective in tuning the polymer surface into hydrophobicity and hydrophilicity, respectively. Such changes in the surface

wettability can be attributed to the variation of both surface roughness and surface chemistry induced by the plasma [40].

2.3 Materials and Fabrication

A typical fabrication process is schematically illustrated in Figure 2. Biocompatible Parylene-C thin films were prepared through vacuum chemical vapor deposition (CVD) on 2-inch silicon wafers using a PDS 2010 Labcoter® 2 (Specialty Coating Systems). A thickness of ~2 μm was deposited and verified by a profilometer. After that, the mixture of PDMS pre-polymer (Dow Corning Sylgard® 184) and curing agent (10:1 by weight) was degassed in a vacuum chamber, spun onto the Parylene-C coated surfaces at 5,000 rpm for 40 s, and then baked at 110 °C for 10 min, in order to obtain PDMS thin films with a thickness of approximately 10 μm. Subsequently, SF_6 plasma was applied to treat the PDMS surface for 40 s with a flow rate of 20 sccm and an RF power of 100 W, using a plasma etcher (PX-250, March Instruments). This SF_6 plasma treatment converted the PDMS substrate to a super hydrophobic surface. After that, photoresist S1813 (Microposit™) was spin-coated at 2,000 rpm for 40 s and baked at 110 °C for 1 min on a hot plate. Through conventional photolithography, the photoresist was patterned to expose openings on substrates as the target positions for microlenses. For the proof-of-concept, a 200 × 200 array of circular patterns with a diameter of 120 μm and a pitch of 250 μm was designed and utilized as a photomask. After the UV exposure and the following development, an O_2 plasma treatment was carried out for 40 s with a flow rate of 15 sccm and an RF power of 100 W, in order to switch the wettability of the exposed PDMS surface from hydrophobicity into hydrophilicity. It is noteworthy that such a brief and low-powered plasma treatment led to an increased surface roughness of only ~2 nm, and thus the substrate exhibited little topological variation. After the removal of the remaining photoresist, PDMS substrates with non-uniform wettability were achieved. Thin SU-8 films (MicroChem Corp.) were immediately spun onto the plasma pre-patterned substrates to avoid the recovery of hydrophilic PDMS regions in air. The high transparency of SU-8 at visible wavelengths makes it suitable for integrated

optical applications [13]. A series of SU-8 3000 photoresists were prepared to contain 30, 40, 50, and 60 wt.% resin by diluting the resin in the SU-8 thinner (cyclopentanone, MicroChem Corp.), followed by spin-coating at 1,000 rpm for 40 s to obtain SU-8 thin films with approximately 6, 10, 20, and 30 μm thickness, respectively.

Figure S1 shows the experimental setup of the vapor-induced dewetting process. The samples were placed into the vapor atmosphere of cyclopentanone to initiate dewetting. They were elevated by a small support to avoid contact with the solvent liquid. This process was performed at room temperature, except when specifically mentioned, in which case a hot plate was utilized to heat the liquid of cyclopentanone. The progression of dewetting was monitored through a stereo microscope (AmScope) equipped with a CCD camera. After the completion of dewetting, the samples were removed from the setup and cured by exposing the dewetted patterns to UV for 1 min.

2.4 Characterization

Water contact angle (WCA) measurement was conducted to confirm the wettability of untreated and plasma-treated PDMS surfaces with a contact angle analysis system (VCA 2000, AST Products, Inc.). The morphology of microlens arrays was inspected by a scanning electron microscope (SEM, Hitachi S-4700 II FESEM), and the lens curvature was measured by a stylus surface profiler (Dektak^3, Veeco Instruments, Inc.). Ten microlenses randomly selected from each array were scanned in order to verify the uniformity. The optical characterization was performed by examining the imaging capabilities of microlenses under an optical microscope (Eclipse LV100, Nikon).

III. Results

3.1 WCA Measurement

The surface wettability on PDMS substrates was inspected by measuring the WCAs before and after the plasma treatments. Prior to any treatments, the intact PDMS surface exhibited a WCA of 109.3 ± 0.4°. The hydrophobicity of the PDMS was enhanced through the SF_6 plasma treatment, with a WCA of 155.8 ± 1.6°. The following O_2 plasma treatment led to a complete inversion of the wettability of the PDMS surface where a complete wetting (WCA ~ 0°) was observed. These findings are consistent with previously reported results for surface wettability modification by SF_6 and O_2 plasmas [40].

3.2 Progression of Dewetting

Figure 3 presents a sequence of microscopic images to show the evolution of the morphology of a ~20-μm-thick SU-8 liquid film during the vapor-induced, room temperature dewetting process. (For a time-lapse view of dewetting process, see Movie S1 in the Supplementary Information.) It can be seen that dewetting originated from the position where defects or impurities existed, which could be caused by the contact with dusts in the ambient environment. They can also be introduced by gently pointing the surface with the tip of tweezers or blowing with nitrogen gas. It is remarkable that although such nucleation points are necessary for initiation of dewetting, too many of them should be avoided in order to maintain the uniformity of microlenses. As shown in Figure 3(a), the initially smooth thin film broke up and a circular dry hole was formed, which can be attributed to the rupture mechanism of "heterogeneous nucleation" due to a microscale wettability contrast [17, 41, 42]. Such instability was manifested after 30 s exposure to the solvent vapor. After the nucleation, the dry hole grew laterally with time to form a dewetted region with a three-phase contact line progressively expanding ahead of the hole (Figure 3(b)). This was owing to the local curvature around the edge of the hole, which was higher than that on the surrounding flat film surface, resulting in a continuing net flux outwards from the edge and a retraction of the contact line [18]. When the contact line reached a hydrophilic spot, it pinned on that spot with an obvious distortion (Figure 3(c)). Such distortion increased as the contact line continued to expand, until a breakup eventually occurred around the hydrophilic spot. It has been reported that the amplitude of

distortion is proportional to the size of the wetting spot [43]. As a result, a certain amount of SU-8 polymer liquid was confined within the hydrophilic area, forming an individually isolated micro-droplet. The deformation of the contact line gradually relaxed after the breakup. The morphology of the dewetted microlens array was clearly observed under the microscope after 4 min. The borders of the SU-8 droplets matched exactly to the boundary of the hydrophilic spots on PDMS resulting from the selective surface pre-patterning through SF_6 and O_2 plasma treatments, which is in good agreement with the simulation. At the late stage, the neighboring dewetted regions coalesced as their contact lines overlapped once on contact with each other. The whole dewetting process lasted for 7 min before completion. After that, no further change was observed in the overall morphology.

3.3 Surface Morphology

The as-fabricated SU-8 microlens arrays were observed through SEM, as presented in Figure 4(a) and (b), which demonstrates the uniformity of microlens array over the entire PDMS surface. It is worth noting that the imperfect lens profile is caused mainly by the limited resolution of transparency masks employed in the photolithography process, which can be improved by using high resolution photomasks. SEM images also showed the existence of secondary droplets (also known as satellite droplets) close to each main droplet (i.e., microlens) in the array. Such secondary droplets were generated during the contact line breakup and their formation has been found to be a common phenomenon, which is strongly correlated to the ratio of characteristic instability wavelength for breakup to the length scale of the distortion [43, 44]. In addition, their location implies the information about the motion history of dewetting.

In most work of this paper, such secondary SU-8 droplets have not been cleared away because it seemed their existence had no obvious influence on the optical performance of microlens arrays. However, it is helpful to point out that they can be removed through an additional photolithography process, since SU-8 is a negative photoresist material which is patternable by the UV light. An experiment was carried out for

the demonstration. After the completion of dewetting process, a sample with dewetted structures was exposed to UV for 3 min with the same photomask aligned. In this case, upon exposure only main SU-8 microlenses became insoluble to the developer, while the secondary SU-8 droplets were unexposed and remained soluble to the developer. Subsequently, the sample was immersed into the SU-8 developer and a cotton-tipped swab was used to wipe the surface gently to expedite the development. After 20 sec, the sample was moved out of the developer and rinsed by isopropanol and deionized water before blow-drying with nitrogen. Optical micrographs of the surface morphology before and after this process are presented in Figure 4(c) and (d), respectively, which clearly shows that the secondary SU-8 droplets have been successfully removed.

3.4 Curvature of Microlenses

The curvature of microlenses was characterized in terms of contact angle, which was determined by the following equation:

$$\theta = 2\arctan(\frac{2h}{d}), \tag{6}$$

where d is the diameter of the base, h is the height of the droplet, and θ is the contact angle. The diameter and the height of microlenses were measured by the surface profiler, as shown in Figure 5.

The influences of the initial film thickness and the processing temperature on the microlens curvature were also investigated and plotted, as shown in Figure 6. In order to study the temperature dependence of vapor-induced dewetting, the experimental setup was placed on a hot plate with various setting temperatures (T = 40 °C, 60 °C and 80 °C), as illustrated in Figure S1. It is evident from Figure 6 that the microlens curvature is strongly correlated to the processing temperature but nearly independent of the initial film thickness. The contact angle increases from ~27° to ~47° as the processing temperature rises from 20 °C (i.e., room temperature) to 80 °C. On the other hand, other processing parameters, such as the

amounts of resin and thinner in SU-8 film, have a negligible impact on the dewetting process compared to the temperature.

We have also demonstrated that the surface property of PDMS was not affected significantly by cyclopentanone even at 80 °C, as evidenced by the visual inspection under a microscope, and the WCA measurement (Fig. S2) where the WCA of the treated PDMS surface (110.1 ± 1.0°) was close to that of the pristine PDMS surface (109.3 ± 0.4°).

3.5 Optical Characterization

The imaging ability of as-fabricated microlens arrays was evaluated as the optical characterization. After the completion of dewetting, the self-organized SU-8 microlens arrays, along with the PDMS/Parylene-C substrates, were carefully peeled off and immediately transferred onto microscope slides. A printed photomask with a black letter "S" was used as the projection template to be imaged for the demonstration. Figure 7(a) schematically illustrates the testing setup, in which a microlens array, carried by a microscope slide, was positioned on the sample stage of an optical microscope and then illuminated from below through the projection template. The separation between the microlens array and the projection template, which is commonly referred to as the object distance (u), is adjustable. Both the lens material (SU-8) and structural material (PDMS and Parylene-C) employed in our experiment have high optical transparency at visible wavelengths (400 nm to 800 nm) so as to reduce the light absorption by the polymers. The light passing through the template was imaged by the microlenses on the image plane and then projected through the objective lens of the microscope for observation. Figure 7(b) displays a projected image captured by an equipped CCD camera. An array of miniaturized letters "S" was observed over an SU-8 microlens array with an object distance of 11 mm. The images are inverted, real, and reduced in size with respect to the object (i.e., the projection template), which demonstrates the converging function of microlenses and their capability as optical elements.

The optical characteristics of the microlenses were further studied using the lens equation, which provides the quantitative relationship among the object distance (u), the image distance (v), and the focal length (f), as given below:

$$\frac{1}{u}+\frac{1}{v}=\frac{1}{f}. \tag{7}$$

The magnification factor (M), defined as the ratio of the size of the image (i) to the size of the object (o), can be expressed as follows:

$$M=\frac{i}{o}=\frac{v}{u}. \tag{8}$$

Substitution of Eq. (8) into Eq. (7) yields:

$$f=u\cdot\frac{M}{M+1}. \tag{9}$$

Another important optical parameter, the numerical aperture (NA), is a function of the diameter of the base (d) and the focal length (f), expressed by:

$$\mathrm{NA}=\frac{d}{2f}. \tag{10}$$

Eqs. (9) and (10) were applied to evaluate the focal length and the numerical aperture of microlenses by measuring the object distance and the magnification factor. For convenience, a calibration slide with 100 μm divisions was used for the observation in this experiment. At least ten microlenses randomly selected from each array were measured and the average was taken. Table I summarizes the measured geometrical and optical properties of SU-8 microlenses with typical curvatures, which were fabricated through vapor-induced dewetting at various processing temperatures. The focal length decreased from 359.4 μm to 219.2 μm and the numerical aperture increased from 0.166 to 0.273 with an increased contact angle from 27.0 ° to 46.1 °.

TABLE I
GEOMETRICAL AND OPTICAL PROPERTIES OF SU-8 MICROLENSES WITH TYPICAL CURVATURES

t (μm)	T (°C)	d (μm)	h (μm)	θ (°)	f (μm)	NA
20	20	119.1±1.8	14.3±0.2	27.0±0.5	359.4±7.3	0.166±0.002
20	40	119.0±0.2	17.8±0.3	33.3±0.6	281.3±9.1	0.212±0.005
20	60	119.4±1.2	22.0±0.3	40.5±0.7	260.8±7.0	0.228±0.003
20	80	119.6±1.2	25.4±0.3	46.1±0.4	219.2±6.6	0.273±0.002

t - approximate initial film thickness; T - processing temperature; d - diameter of the base; h - height of the microlens; θ - contact angle; f - focal length; NA - numerical aperture.

IV. Discussion

One of the advantages in our experiment is the activation of dewetting at room temperature, which can be attributed to the exposure to the solvent vapor. For comparison, we have also investigated the dewetting process without solvent vapor exposure on chemically patterned PDMS substrates that were prepared in exactly the same way as described previously. In this case, no dewetting occurred at room temperature even after two months. The experimental setup illustrated in Figure S1, but without the presence of the solvent, was employed to find out the approximate dewetting temperature. The temperature of the hot plate was controlled such that it started from 20 °C with an increment of 5 °C per hour, until the occurrence of dewetting. The experiment showed that the rupture started to appear at 50, 55, 55, and 60 °C on SU-8 thin films with initial thicknesses of approximately 6, 10, 20, and 30 μm, respectively. In sharp contrast, by exposure to the solvent vapor, dewetting can be rapidly triggered at room temperature on all the samples with various initial film thicknesses. Such a big difference can be primarily attributed to the activation of glass transition of SU-8 at room temperature owing to the presence of the solvent vapor [45]. The evaporated gas molecules of cyclopentanone can be absorbed into the SU-8 layer and thus the film viscosity is lowered. Such adsorption also weakens the interaction between the SU-8 film and the PDMS substrate. As a result, SU-8 polymer chains obtain enough mobility to be able to slide on the substrate even at room temperature.

The achievement of self-organization of dewetted microlenses has proved that the heterogeneity in surface chemistry could act as an ideal template to control the dewetting dynamics. In our experiment, the

three-phase contact line displays an anisotropic receding speed once on contact with a hydrophilic spot. In fact, unlike the super-hydrophobic surface, the super-hydrophilic PDMS area has a higher surface energy, giving rise to a negative value of the effective Hamaker constant [35]. Therefore, the van der Waals force tends to stabilize the surface, which means that, theoretically, the SU-8 thin film does not dewet on the super-hydrophilic PDMS substrate. This is in accordance with our observation in which the SU-8 polymer liquid adhered onto the hydrophilic PDMS surface and was prevented from removal by dewetting. As a consequence, the contact line was pinned at the hydrophobic-hydrophilic boundary but still receded across the hydrophobic domain. This mechanism of pattern-directed dewetting is analogous to that observed on topologically heterogeneous substrates [23], except that it derives from the disjoining pressure due to the wettability contrast rather than from the capillary pressure due to the local curvature. As the contact line shifted along the hydrophobic-hydrophilic boundary, the distortion caused a neck to be generated on the side away from the wetting spot. The increased azimuthal curvature at the neck enhanced the pressure locally, drove the flow away and eventually led to a pinch-off, which belongs to the breakup mechanism of end-pitching [46]. With continuous recession of the contact line and the repetitive occurrence of end-pitching, the morphology of the microlens array has been successfully generated. The conclusion can be drawn that the heterogeneity in surface wettability can effectively guide thin film instabilities and provide control on the dewetted morphology.

In addition, we have also demonstrated that the templated dewetting on chemically patterned substrates is widely applicable to creating ordered and even complex micro-structures with various geometries. Figure 8(a)-(c) presents optical micrographs of a series of periodic SU-8 patterns that were prepared by our method, including parallel strips, an array of squares, and an array of “Spartans” logos on PDMS substrates. Furthermore, our dewetting process is applicable to different substrates. As an example, SU-8 microlens arrays were successfully generated on a ~2-μm-thick chemically patterned Parylene-C thin film through vapor-induced, room temperature dewetting, as shown in Figure 8(d). These microlenses show an average contact angle of 2.8 ± 0.4°, which is different from the contact angles of microlenses dewetted on

PDMS substrates, suggesting the influence of surface tension and surface chemistry on the dewetting process.

The optical properties of microlens arrays are of great importance in their optical performance for various applications. For example, microlenses with larger NAs show a stronger ability to gather light and resolve details. The fill factor of microlens arrays is crucial for low noise and high throughput of optical signal. Therefore, an emphasis will be placed on the improvement of such optical properties in future study. One of the promising approaches is to select a liquid material with desired surface tension and refractive index, which can influence both lens curvature and optical property. Appropriate adjustment on the shapes of the base of microlenses (such as hexagons [10]) and increase of their density on the photomask could also be helpful for the producing microlens arrays with high fill factors.

V. Conclusion

In summary, this study has demonstrated the efficacy of a vapor-induced dewetting method for the fabrication of microlens arrays on chemically patterned substrates. The surface heterogeneity, arising from the selective SF_6 and O_2 plasma treatments, acted as an ideal template to control the dewetting dynamics. The dewetted SU-8 droplets were spontaneously organized on O_2-plasma-treated hydrophilic spots to form well-aligned microlens arrays. The exposure to the solvent vapor allows for the initialization of dewetting at room temperature. The microlens curvature is strongly correlated to the processing temperature, but nearly independent of the initial film thickness. The imaging ability of the as-fabricated microlenses has shown that a range of optical properties can be obtained. Our method provides a versatile and effective route for engineering periodic micro-scale structures over large areas for applications in micro-electronic and optical devices. To further improve the optical performance of microlens arrays, an investigation on the pursuit of excellent optical properties, including large NAs and high fill factors, will be carried out in the future study.

Acknowledgment

This work was supported by the Electrical, Communications and Cyber Systems Division of the National Science Foundation under the Award Number ECCS-1055269.

References

[1] M. Sieler, P. Schreiber, and A. Bräuer, "Microlens array based LCD projection display with software-only focal distance control," in *Int. Conf. SPIE*, Aug. 2013, pp. 86430B-1–86430B-8.

[2] J. Arai, H. Kawai, and F. Okano, "Microlens arrays for integral imaging system," *Applied Optics,* vol. 45, no. 36, pp. 9066–9078, Dec. 2006.

[3] M. Martinez-Corral, B. Javidi, R. Martinez-Cuenca, and G. Saavedra, "Integral imaging with improved depth of field by use of amplitude-modulated microlens arrays," *Applied Optics,* vol. 43, no. 31, pp. 5806–5813, Nov. 2004.

[4] M. S. Kim, K. W. Jo, J. H. Lee, K. B. Song, E. K. Kim, and K. H. Park, "Self-aligned microlens fabricated on the sidewall of 45°-angled optical fiber for NSOM illumination system," in *Int. Conf. Optical MEMS*, Aug. 2003, pp. 18–19.

[5] L. P. Zhao, N. Bai, X. Li, L. S. Ong, Z. P. Fang, and A. K. Asundi, "Efficient implementation of a spatial light modulator as a diffractive optical microlens array in a digital Shack-Hartmann wavefront sensor," *Applied Optics,* vol. 45, no. 1, pp. 90–94, Jan. 2006.

[6] N. Grossman, V. Poher, M. S. Grubb, G. T. Kennedy, K. Nikolic, B. McGovern*, et al.*, "Multi-site optical excitation using ChR2 and micro-LED array," *Journal of Neural Engineering,* vol. 7, no. 1, pp. 016004-1–016004-13, Feb. 2010.

[7] K. Totsu, K. Fujishiro, S. Tanaka, and M. Esashi, "Fabrication of three-dimensional microstructure using maskless gray-scale lithography," *Sensors and Actuators A-Physical,* vol. 130–131, pp. 387–392, Aug. 2006.

[8] M. Manevich, M. Klebanov, V. Lyubin, J. Varshal, J. Broder, and N. P. Eisenberg, "Gap micro-lithography for chalcogenide micro-lens array fabrication," *Chalcogenide Letters,* vol. 5, no. 4, pp. 61–64, Apr. 2008.

[9] S. Y. Hung, C. K. Chao, T. H. Lin, and C. P. Lin, "Applying ANN/GA algorithm to optimize the high fill-factor microlens array fabrication using UV proximity printing process," *Journal of Micromechanics and Microengineering,* vol. 15, no. 12, pp. 2389–2397, Dec. 2005.

[10] D. Wu, S. Z. Wu, L. G. Niu, Q. D. Chen, R. Wang, J. F. Song*, et al.*, "High numerical aperture microlens arrays of close packing," *Applied Physics Letters,* vol. 97, no. 3, pp. 031109-1–031109-3, Jul. 2010.

[11] J. Y. Kim, N. B. Brauer, V. Fakhfouri, D. L. Boiko, E. Charbon, G. Grutzner*, et al.*, "Hybrid polymer microlens arrays with high numerical apertures fabricated using simple ink-jet printing technique," *Optical Materials Express,* vol. 1, no. 2, pp. 259–269, Jun. 2011.

[12] J. Y. Kim, K. Pfeiffer, A. Voigt, G. Gruetzner, and J. Brugger, "Directly fabricated multi-scale microlens arrays on a hydrophobic flat surface by a simple ink-jet printing technique," *Journal of Materials Chemistry,* vol. 22, no. 7, pp. 3053–3058, 2012.

[13] V. Fakhfouri, N. Cantale, G. Mermoud, J. Y. Kim, D. Boiko, E. Charbon*, et al.*, "Inkjet printing of SU-8 for polymer-based MEMS a case study for microlenses," in *21st Int. Conf. MEMS*, Jan. 2008, pp. 407–410.

[14] E. Roy, B. Voisin, J. F. Gravel, R. Peytavi, D. Boudreau, and T. Veres, "Microlens array fabrication by enhanced thermal reflow process: Towards efficient collection of fluorescence light from microarrays," *Microelectronic Engineering,* vol. 86, no. 11, pp. 2255–2261, Nov. 2009.

[15] R. van Hameren, P. Schon, A. M. van Buul, J. Hoogboom, S. V. Lazarenko, J. W. Gerritsen*, et al.*, "Macroscopic hierarchical surface patterning of porphyrin trimers via self-assembly and dewetting," *Science,* vol. 314, no. 5804, pp. 1433–1436, Dec. 2006.

[16] A. M. Higgins and R. A. L. Jones, "Anisotropic spinodal dewetting as a route to self-assembly of patterned surfaces," *Nature,* vol. 404, no. 6777, pp. 476–478, Mar. 2000.

[17] L. J. Xue and Y. C. Han, "Pattern formation by dewetting of polymer thin film," *Progress in Polymer Science,* vol. 36, no. 2, pp. 269–293, Feb. 2011.

[18] C. V. Thompson, "Solid-state dewetting of thin films," *Annual Review of Materials Research,* vol. 42, pp. 399–434, Aug. 2012.

[19] D. Bonn, J. Eggers, J. Indekeu, J. Meunier, and E. Rolley, "Wetting and spreading," *Reviews of Modern Physics,* vol. 81, no. 2, pp. 739–805, Apr.–Jun. 2009.

[20] R. Seemann, S. Herminghaus, and K. Jacobs, "Gaining control of pattern formation of dewetting liquid films," *Journal of Physics-Condensed Matter,* vol. 13, no. 21, pp. 4925–4938, May 2001.

[21] G. Reiter, "Dewetting of thin polymer films," *Physical Review Letters,* vol. 68, no. 1, pp. 75–78, Jan. 1992.

[22] R. Mukherjee, D. Bandyopadhyay, and A. Sharma, "Control of morphology in pattern directed dewetting of thin polymer films," *Soft Matter,* vol. 4, no. 10, pp. 2086–2097, 2008.

[23] R. B. Xing, C. X. Luo, Z. Wang, and Y. C. Han, "Dewetting of polymethyl methacrylate on the patterned elastomer substrate by solvent vapor treatment," *Polymer,* vol. 48, no. 12, pp. 3574–3583, Jun. 2007.

[24] B. Yoon, H. Acharya, G. Lee, H. C. Kim, J. Huh, and C. Park, "Nanopatterning of thin polymer films by controlled dewetting on a topographic pre-pattern," *Soft Matter,* vol. 4, no. 7, pp. 1467–1472, 2008.

[25] A. Verma and A. Sharma, "Enhanced self-organized dewetting of ultrathin polymer films under water-organic solutions: Fabrication of sub-micrometer spherical lens arrays," *Advanced Materials,* vol. 22, no. 46, pp. 5306–5309, Dec. 2010.

[26] A. Sehgal, V. Ferreiro, J. F. Douglas, E. J. Amis, and A. Karim, "Pattern-directed dewetting of ultrathin polymer films," *Langmuir,* vol. 18, no. 18, pp. 7041–7048, Sep. 2002.

[27] D. Julthongpiput, W. H. Zhang, J. F. Douglas, A. Karim, and M. J. Fasolka, "Pattern-directed to isotropic dewetting transition in polymer films on micropatterned surfaces with differential surface energy contrast," *Soft Matter,* vol. 3, no. 5, pp. 613–618, 2007.

[28] B. J. Brasjen, H. Gu, and A. A. Darhuber, "Dewetting of thin liquid films on chemically patterned substrates: front propagation along narrow lyophobic stripes and stripe arrays," *Microfluidics and Nanofluidics,* vol. 14, no. 3–4, pp. 669–682, Mar. 2013.

[29] Z. X. Zhang, Z. Wang, R. B. Xing, and Y. C. Han, "Patterning thin polymer films by surface-directed dewetting and pattern transfer," *Polymer,* vol. 44, no. 13, pp. 3737–3743, Jun. 2003.

[30] K. Kargupta, R. Konnur, and A. Sharma, "Instability and pattern formation in thin liquid films on chemically heterogeneous substrates," *Langmuir,* vol. 16, no. 26, pp. 10243–10253, Dec. 2000.

[31] K. Kargupta and A. Sharma, "Creation of ordered patterns by dewetting of thin films on homogeneous and heterogeneous substrates," *Journal of Colloid and Interface Science,* vol. 245, no. 1, pp. 99–115, Jan. 2002.

[32] K. L. Lai, S. F. Hsiao, M. H. Hon, and I. C. Leu, "Patterning of polystyrene thin films by solvent-assisted imprint lithography and controlled dewetting," *Microelectronic Engineering,* vol. 94, pp. 33–37, Jun. 2012.

[33] C. X. Luo, R. B. Xing, and Y. C. Han, "Ordered pattern formation from dewetting of polymer thin film with surface disturbance by capillary force lithography," *Surface Science,* vol. 552, no. 1–3, pp. 139–148, Mar. 2004.

[34] S. Costacurta, P. Falcaro, L. Malfatti, D. Marongiu, B. Marmiroli, F. Cacho-Nerin*, et al.*, "Shaping mesoporous films using dewetting on X-ray pre-patterned hydrophilic/hydrophobic layers and pinning effects at the pattern edge," *Langmuir,* vol. 27, no. 7, pp. 3898–3905, Apr. 2011.

[35] L. Xu, A. Sharma, and S. W. Joo, "Dewetting of stable thin polymer films induced by a poor solvent: Role of polar interactions," *Macromolecules,* vol. 45, no. 16, pp. 6628–6633, Aug. 2012.

[36] L. W. Schwartz and R. R. Eley, "Simulation of droplet motion on low-energy and heterogeneous surfaces," *Journal of Colloid and Interface Science,* vol. 202, no. 1, pp. 173–188, Jun. 1998.

[37] A. Oron, S. H. Davis, and S. G. Bankoff, "Long-scale evolution of thin liquid films," *Reviews of Modern Physics,* vol. 69, no. 3, pp. 931–980, Jul. 1997.

[38] T. P. Witelski and M. Bowen, "ADI schemes for higher-order nonlinear diffusion equations," *Applied Numerical Mathematics,* vol. 45, no. 2–3, pp. 331–351, May 2003.

[39] X. P. Bi, N. L. Ward, B. P. Crum, and W. Li, "Plasma-treated switchable wettability of parylene-C surface," in *7th Int. Conf. NEMS*, Mar. 2012, pp. 222–225.

[40] X. P. Bi, B. P. Crum, and W. Li, "Super hydrophobic parylene-C produced by consecutive O_2 and SF_6 plasma treatment," *Journal of Microelectromechanical Systems,* vol. 23, no. 3, pp. 628–635, Jun. 2014.

[41] B. J. Brasjen and A. A. Darhuber, "Dry-spot nucleation in thin liquid films on chemically patterned surfaces," *Microfluidics and Nanofluidics,* vol. 11, no. 6, pp. 703–716, Dec. 2011.

[42] R. Konnur, K. Kargupta, and A. Sharma, "Instability and morphology of thin liquid films on chemically heterogeneous substrates," *Physical Review Letters,* vol. 84, no. 5, pp. 931–934, Jan. 2000.

[43] T. Cubaud, P. Jenffer, and M. Fermigier, "Dewetting of patterned surfaces," in *4th European Coating Symposium*, Oct. 2001, pp. 1–4.

[44] L. W. Schwartz, R. V. Roy, R. R. Eley, and S. Petrash, "Dewetting patterns in a drying liquid film," *Journal of Colloid and Interface Science,* vol. 234, no. 2, pp. 363–374, Feb. 2001.

[45] L. Leibler and K. Sekimoto, "On the sorption of gases and liquids in glassy polymers," *Macromolecules,* vol. 26, no. 25, pp. 6937–6939, Dec. 1993.

[46] G. Ghigliotti, C. F. Zhou, and J. J. Feng, "Simulations of the breakup of liquid filaments on a partially wetting solid substrate," *Physics of Fluids,* vol. 25, no. 7, pp. 072102-1–072102-14, Jul. 2013.

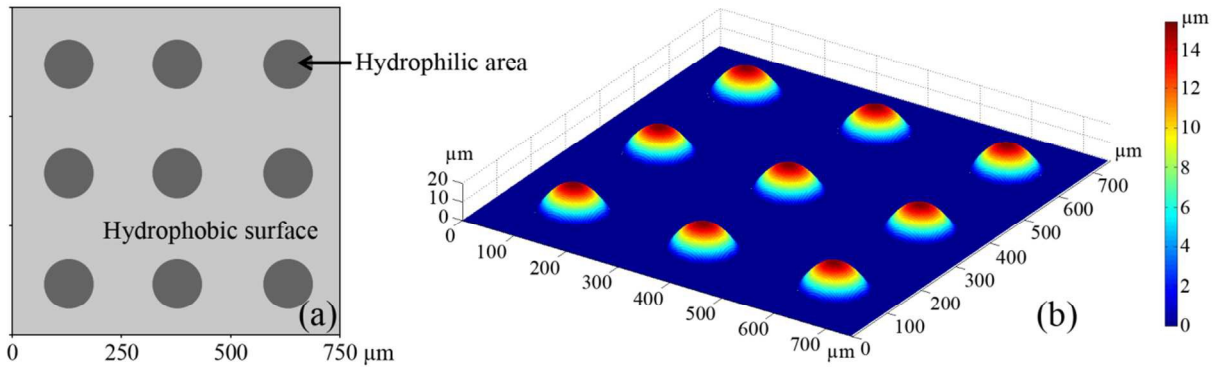

Figure 1. (a) A schematic of the computational domain, which includes a 3 × 3 array of hydrophilic circular patterns on a hydrophobic substrate. Symmetry conditions were applied along all boundaries to simulate an ideal infinite array. (b) 3-D simulation result for the dewetting process. A self-organized microlens array was formed on the final profile, occupying the ordered hydrophilic areas.

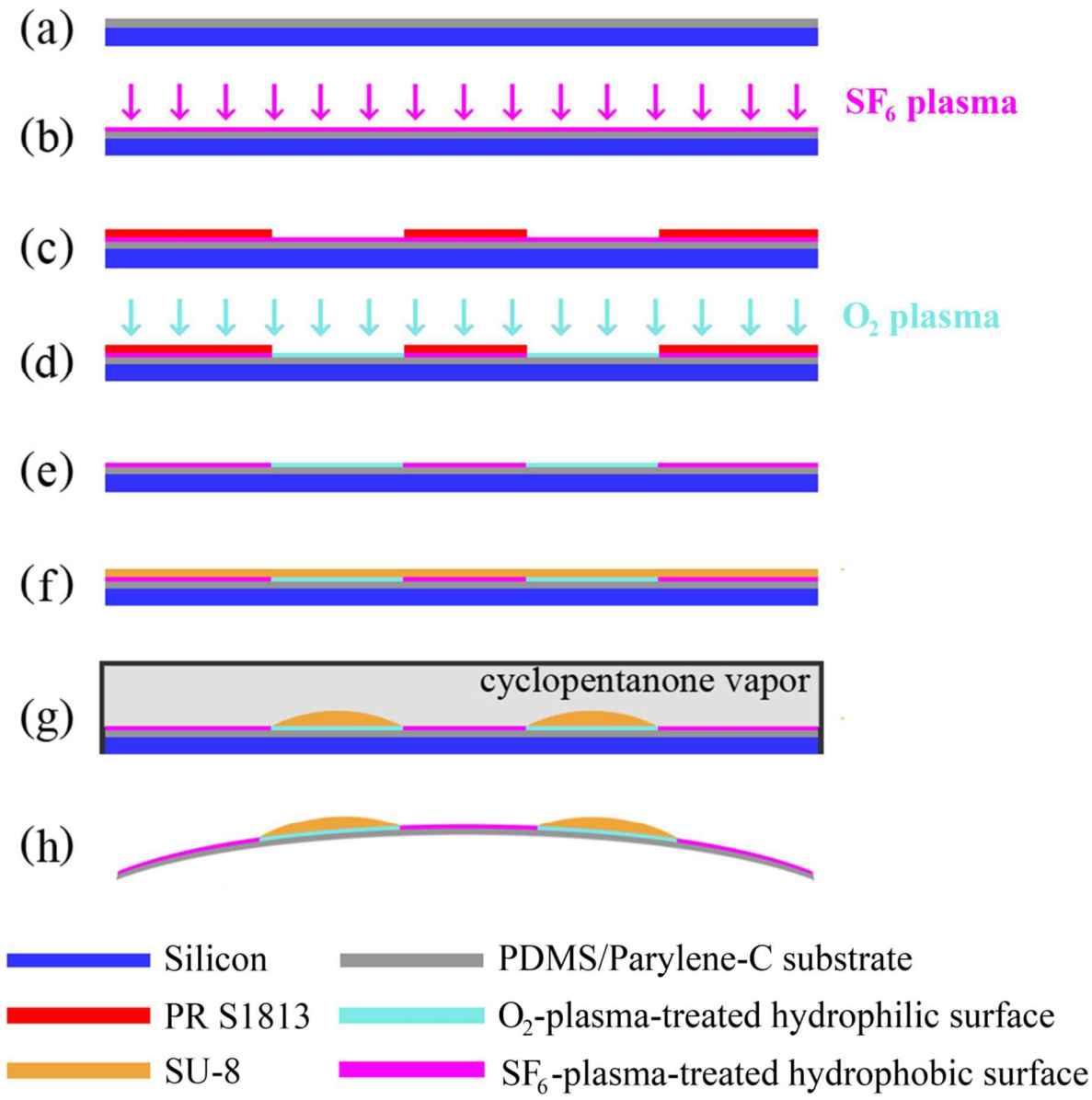

Figure 2. Schematic illustration of the vapor-induced, room temperature dewetting process. (a) Parylene-C deposition and subsequent PDMS spin-coating on a silicon substrate; (b) SF_6 plasma treatment to modify PDMS to a super hydrophobic surface; (c) photolithography; (d) O_2 plasma treatment to switch the wettability of the exposed PDMS surface from hydrophobicity to hydrophilicity; (e) removal of photoresist to obtain a chemically heterogeneous PDMS surface; (f) spin-coating of a thin SU-8 film; (g) initiation of dewetting by placing the sample into the vapor atmosphere of cyclopentanone; (h) achievement of a flexible SU-8 microlens array after peeled off the silicon substrate.

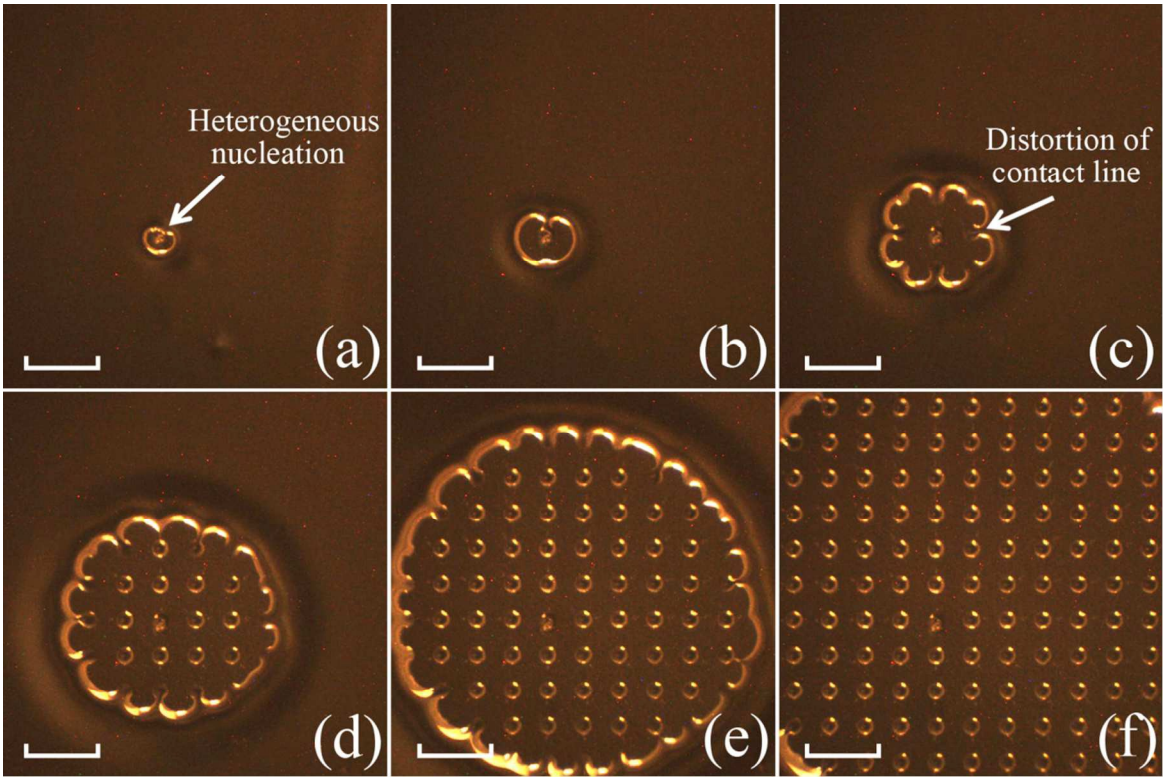

Figure 3. Morphological evolution of a ~20-μm-thick SU-8 liquid film on a chemically patterned PDMS substrate during the vapor-induced, room temperature dewetting process, with a sequence of time intervals: (a) 1 min, (b) 2 min, (c) 3 min, (d) 4 min, (e) 5 min, and (f) 6 min. The scale bars correspond to 500 μm.

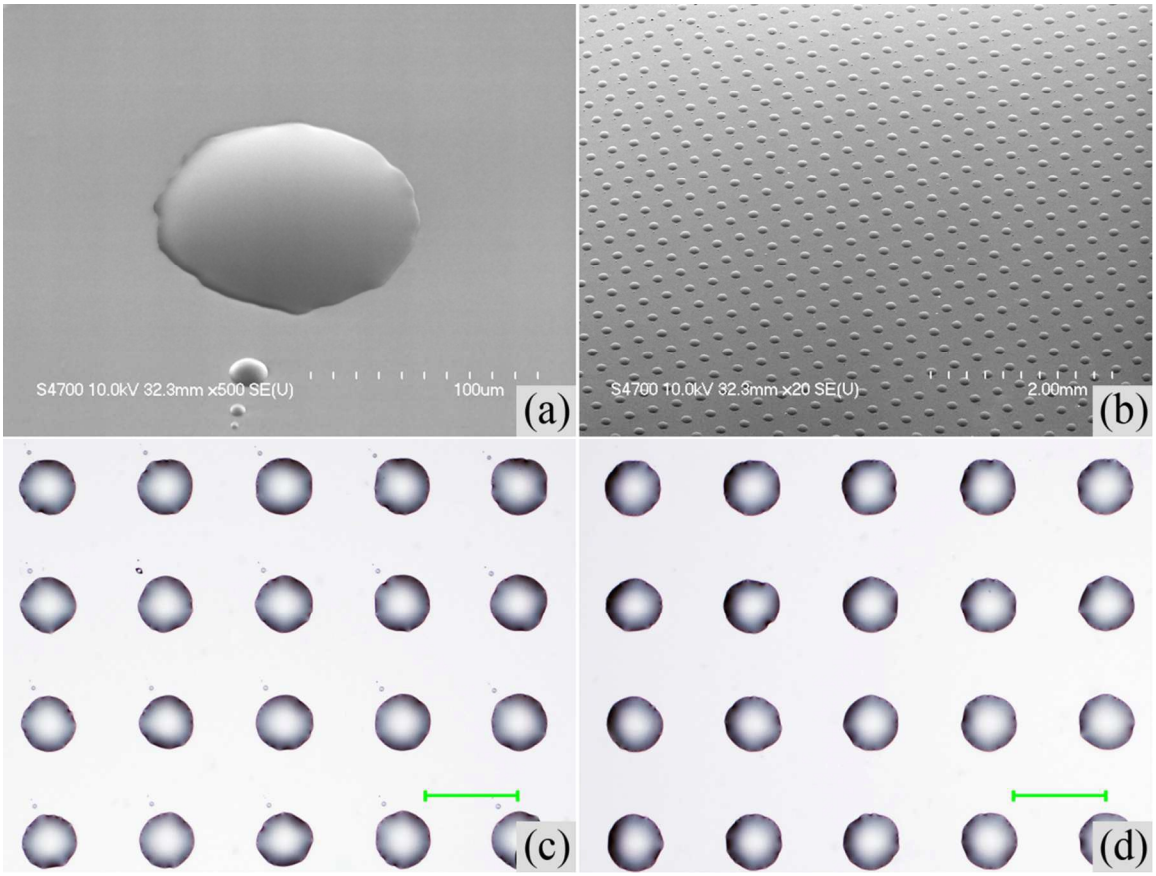

Figure 4. (a)-(b) SEM images of (a) a single SU-8 microlens and (b) an SU-8 microlens array. (c)-(d) Optical micrographs of the surface morphology of an SU-8 microlens array (c) before and (d) after the process for the removal of secondary SU-8 droplets. The microlens array was fabricated through vapor-induced, room temperature dewetting, with an initial film thickness of ~20 μm on a chemically patterned PDMS substrate. The scale bars in (c) and (d) correspond to 200 μm.

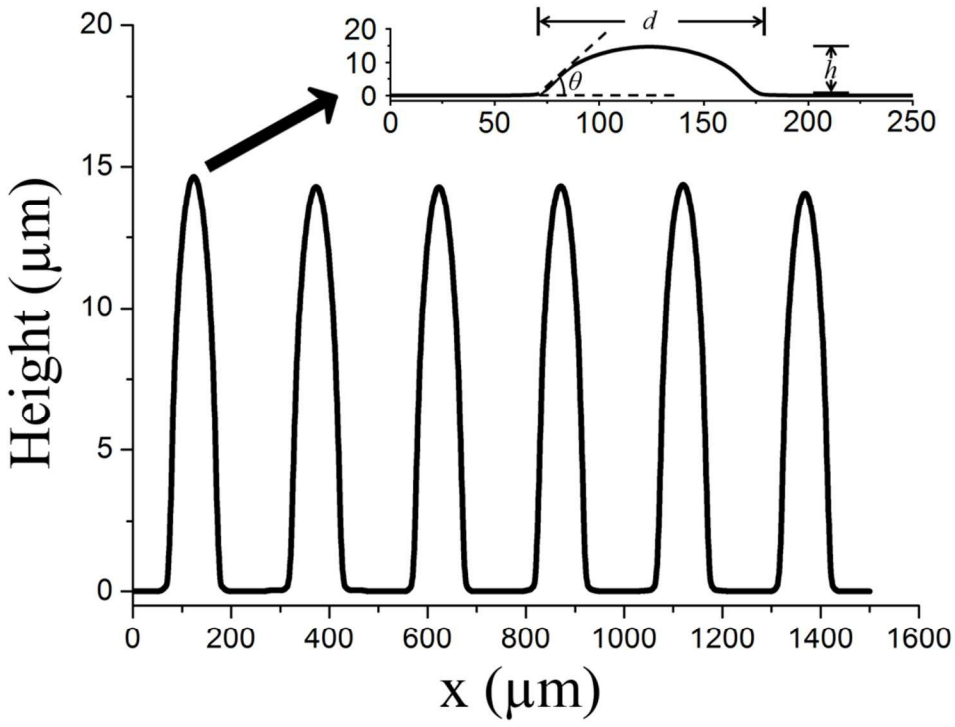

Figure 5. The profilometer measurement of randomly selected SU-8 microlenses, fabricated through vapor-induced, room temperature dewetting, with an initial film thickness of ~20 μm. The inset, showing the profile of the leftmost microlens, illustrates the geometrical relationship among the diameter (d), the height (h) and the contact angle (θ). For example, this microlens has a profile of d = 119.8 μm and h = 14.66 μm, resulting in $\theta = 27.5°$, according to Eq. (6).

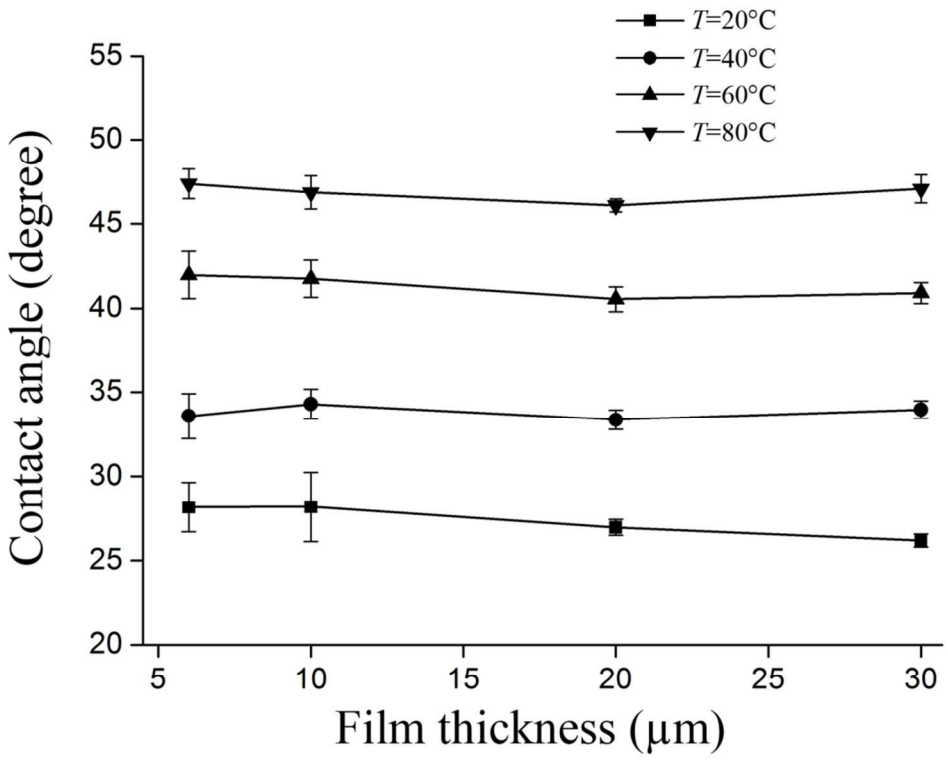

Figure 6. Contact angles of SU-8 microlenses fabricated through vapor-induced dewetting, as a function of the initial film thickness at various processing temperatures.

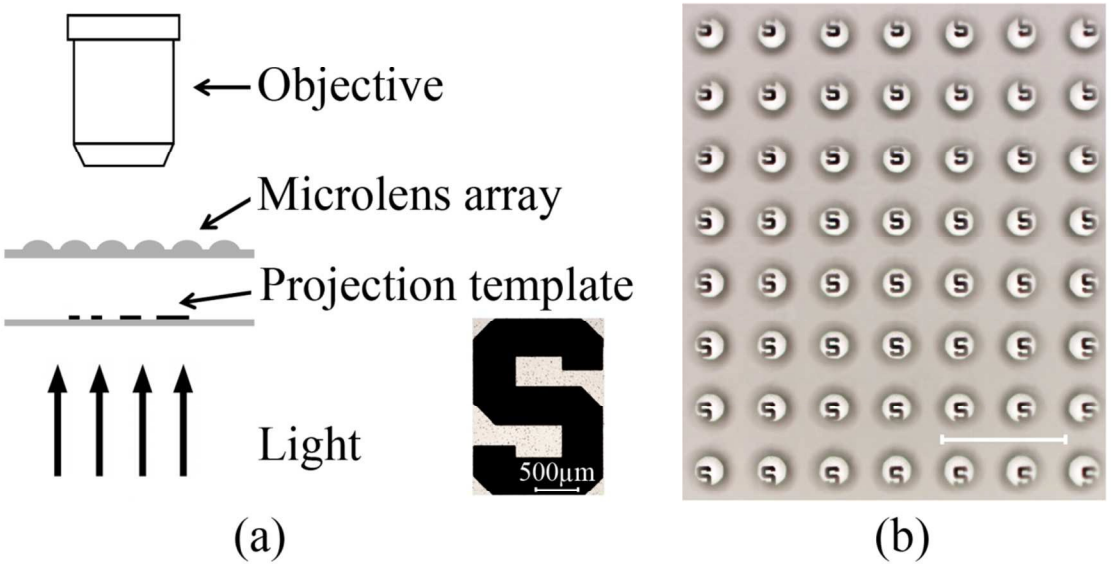

Figure 7. (a) Schematic illustration of the testing setup for the optical characterization of as-fabricated SU-8 microlens arrays. The inset shows an optical micrograph of a photomask with a black letter "S" which was used as the projection template to be imaged for the demonstration. (b) A projected image captured by a CCD camera equipped with the microscope. An array of miniaturized letters "S" was observed over an SU-8 microlens array with an object distance of 11 mm. This microlens array was fabricated through vapor-induced room temperature dewetting, with an initial film thickness of ~20 μm. The scale bars correspond to 500 μm.

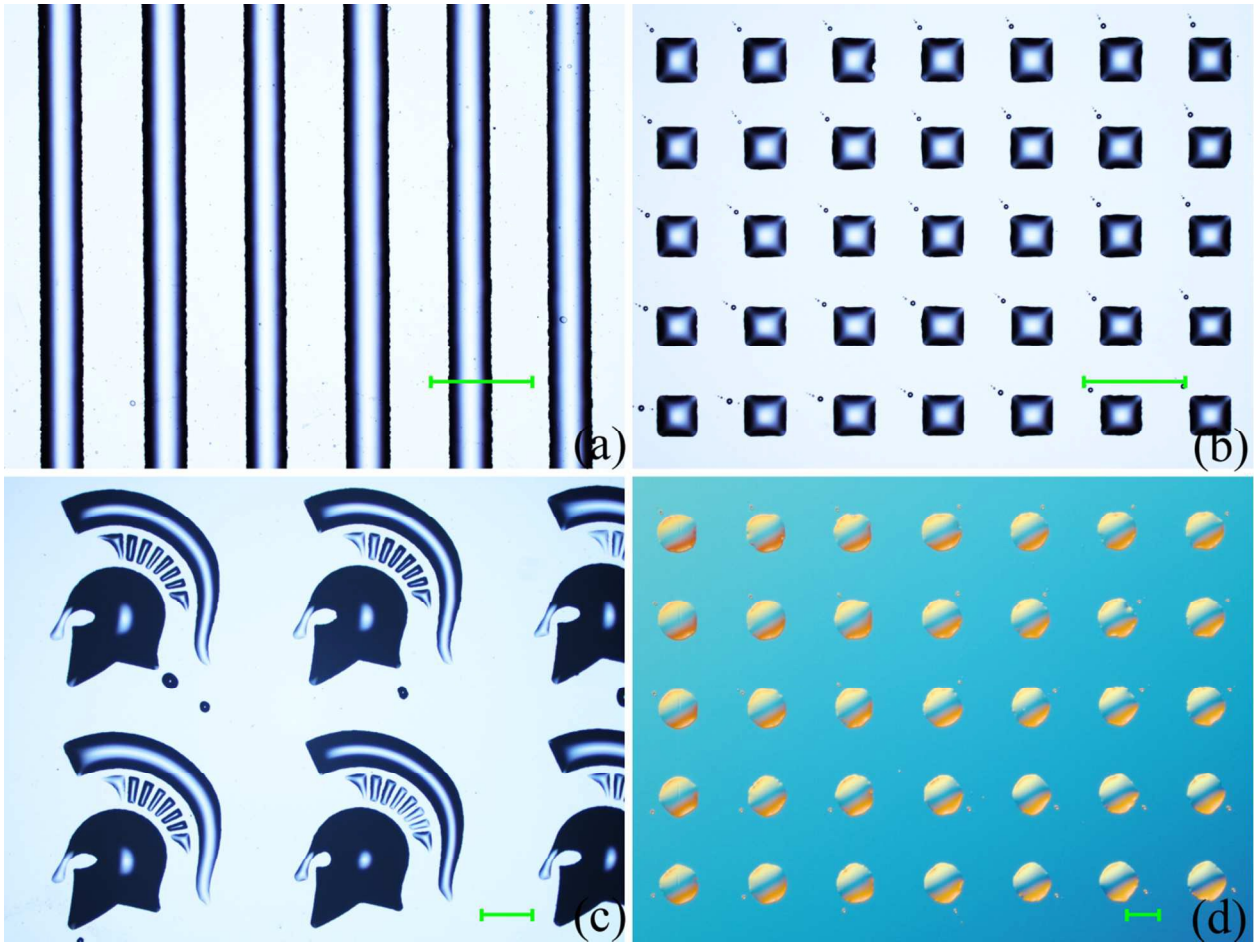

Figure 8. (a)-(c) Optical micrographs of periodic SU-8 micro-patterns on PDMS substrates: (a) parallel strips, (b) an array of squares, and (c) an array of "Spartans" logos. (d) Optical micrograph of an SU-8 microlens array on a Parylene-C substrate. All the micro-structures in this figure were generated through vapor-induced, room temperature dewetting on chemically patterned substrates. The scale bars correspond to 100 μm.

TOC Graphic